NANO LETTERS

Letter

pubs.acs.org/NanoLett

Local Light-Induced Magnetization Using Nanodots and Chiral Molecules

Oren Ben Dor,[†] Noam Morali,[‡] Shira Yochelis,[†] Lech Tomasz Baczewski,[§] and Yossi Paltiel*[,†]

[†]Applied Physics Department and the Center for Nano-Science and Nano-Technology, The Hebrew University of Jerusalem, Jerusalem 91904 Israel

[‡]Department of Physics, The Weizmann Institute of Science, Rehovot 76100, Israel

[§]Institute of Physics Polish Academy of Sciences, Warszawa, Poland

Supporting Information

ABSTRACT: With the increasing demand for miniaturization, nanostructures are likely to become the primary components of future integrated circuits. Different approaches are being pursued toward achieving efficient electronics, among which are spin electronics devices (spintronics). In principle, the application of spintronics should result in reducing the power consumption of electronic devices. Recently a new, promising, effective approach for spintronics has emerged, using spin selectivity in electron transport through chiral molecules. In this work, using chiral molecules and nanocrystals, we achieve local spin-based magnetization generated optically at ambient temperatures. Through the chiral layer, a spin torque can be transferred without permanent charge transfer from the nanocrystals to a thin ferromagnetic layer, creating local perpendicular magnetization. We used Hall sensor configuration and atomic force microscopy (AFM) to measure the induced local magnetization. At low temperatures, anomalous spin Hall effects were measured using a thin Ni layer. The results may lead to optically controlled spintronics logic devices that will enable low power consumption, high density, and cheap fabrication.

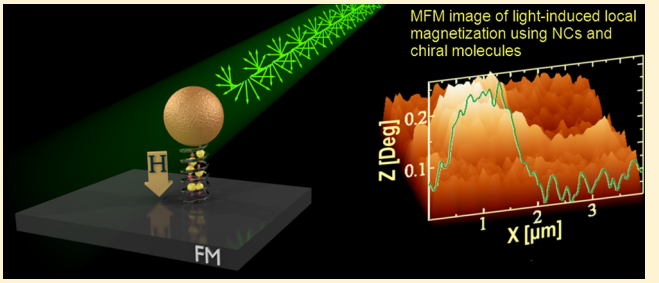

KEYWORDS: *Spin, polarization, local, organic spintronics, memory*

With the increasing demand for scale minimization of integrated circuits, nanostructures are likely to become the primary components of future electronic devices. Further miniaturization and a decrease in power consumption have the highest priority in developing information and communication technology. Different approaches are being pursued toward achieving more efficient and additional down-scalable techniques, among which is the field of spintronics (SPIN TRansport electrONICS).[1,2] In contrast to conventional electronic devices, where the charge of the electron is used for logical operations, as well as for data transmission and storage, in spintronics the spin (the intrinsic angular momentum of the electron) becomes the important degree of freedom. In principle, the application of spintronics should result in more efficient devices, reducing the power consumed in computing and in storing information.

Usually spin-selective electron transport is associated with either magnetized materials or materials that have large spin−orbit coupling. Spin injection, especially injection from a magnetized metal into a semiconductor, suffers from an impedance mismatch,[3] resulting in low spin injection efficiencies.[4] Different strategies that have been used to address this problem[5,6] have been only partially successful. However, an entirely new approach to this problem has emerged in recent work on spin selectivity in electron transport through chiral molecules, specifically, molecules with a helical secondary structure (chiral-induced spin selectivity, CISS effect).[7] Such molecules function as spin filters with a surprisingly high efficiency, even at room temperature (RT).[8] Theoretically, the main approaches to the problem can be categorized as scattering theory[9,10] and quantum transport.[11,12] In both cases, the molecules act as a spin filter or spin polarizer. Such a chiral layer for magnetic memory applications was used to achieve magnetic memory without a permanent magnet.[13] The chiral-based memory device uses a vertical configuration, which limits the function of such devices. Using both vertical and in-plane configurations can open up possibilities for 3D spin logic schemes as well as pave the way for giant magneto-resistant[14] chiral-based devices.

In this work, using chiral molecules and nanocrystals (NCs), we achieved local spin-based magnetization generated optically at ambient temperatures. The locality was obtained both by incorporating the recently developed selective adsorption procedure of the NCs[15] and also by selective illumination using a mask. By optically exciting the NCs, we are able to transfer the spin torque only to a ferromagnetic layer (Figure f1

Received: March 19, 2014
Revised: October 1, 2014

   dx.doi.org/10.1021/nl502391t | *Nano Lett.* XXXX, XXX, XXX−XXX

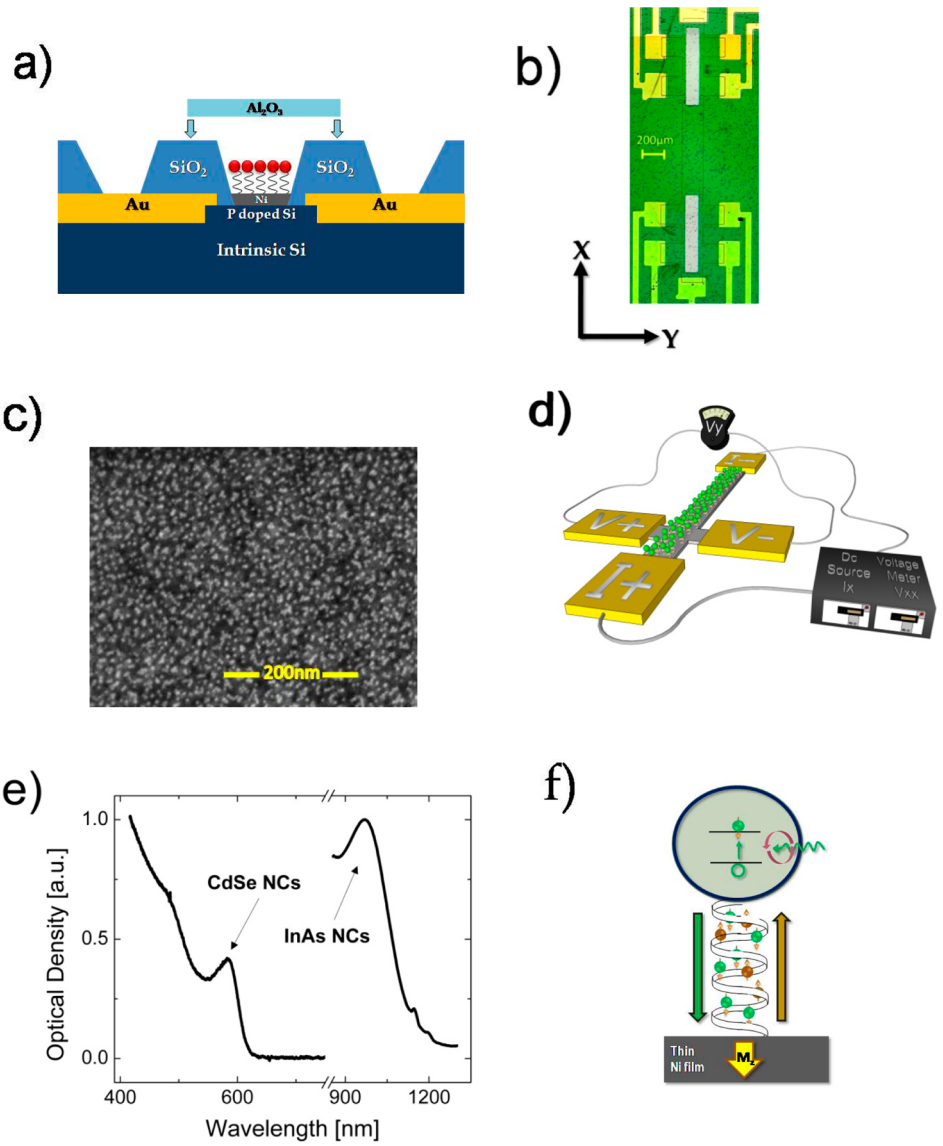

Figure 1. Panels a and d present schematic drawings of the sensors. (a) Schematic cross section of the Si-based sensor. A thin (blue) P-doped Si layer located between two gold (yellow) electrodes. The thin Ni layer is represented in gray and the adsorbed chiral molecules with the InAs NCs on top are shown in red. (b) Optical microscopy top-view image of the Si-based sensor. The conducting channel is along the *X*-axis and the Hall voltage is measured along the *Y*-axis. The sensors' active adsorption windows are presented in gray. (c) SEM image of highly dense 10^{12} NCs/cm^2 CdSe NCs (5 nm diameter) adsorbed on a SAM of AHPA-L molecules attached to the Ni surface. (d) Scheme of the Ni-based device where no effective adsorption areas were used. This device is much simpler to design and needs only 3 fabrication steps. (e) Normalized absorption spectrum of the CdSe and InAs NCs. (f) Illustration of the spin torque transfer mechanism. When the NCs are excited, charges oscillate between the NCs and the Ni surface, passing through the chiral molecules. Owing to the CISS effect, mostly electrons with spin of one type are injected into the Ni layer. The electrons with opposite spins are transferred back in the opposite direction. Both effects together generate spin torque transfer with no charge transport. Exciting light in the right direction of circular polarization can enhance the torque transfer.

f1

1f). At lower temperatures, the anomalous Hall effect (AHE) was measured. Applications for using a simple spin-based logic device as well as a local nuclear magnetic resonance chip are discussed.

Experimental Details and Methods. Local probing of the magnetic field was achieved using different Hall sensor configurations as well as local magnetic AFM (MFM) probing. The Hall effect configuration makes it possible to design a device with an output voltage proportional to the local magnetic field.[16] Three different types of Hall sensors with different ferromagnetic layers were utilized in order to reduce potential artifacts (see details in the Supporting Information). In the first sensor, we magnetized a 5 nm thick Ni layer located on top of a shallow P-doped Si layer (shallow 2D-like electron gas) acting as a Hall sensor (Figure 1a). The second Hall sensor type (namely, the standard Si-based sensor), used phosphor diffusion to n-dope Si layer. This sensor's resistance is smaller and the sensor is more immune to capacity drifts and heating. Lastly, we used a thin 7 nm Ni layer as the Hall conductive layer (Figure 1d). Consequently, the resulting transport in the Ni channel is sensitive to the spin injected into the surface states of the top oxidized layer, which induces spin torque transfer into the Ni channel.[17,18] This sensor is termed the Ni-based Hall sensor throughout this paper. In all types of Hall sensors, Si- and Ni-based sensors, we used various active areas to which molecules and NCs were adsorbed.

dx.doi.org/10.1021/nl502391t | *Nano Lett.* XXXX, XXX, XXX−XXX

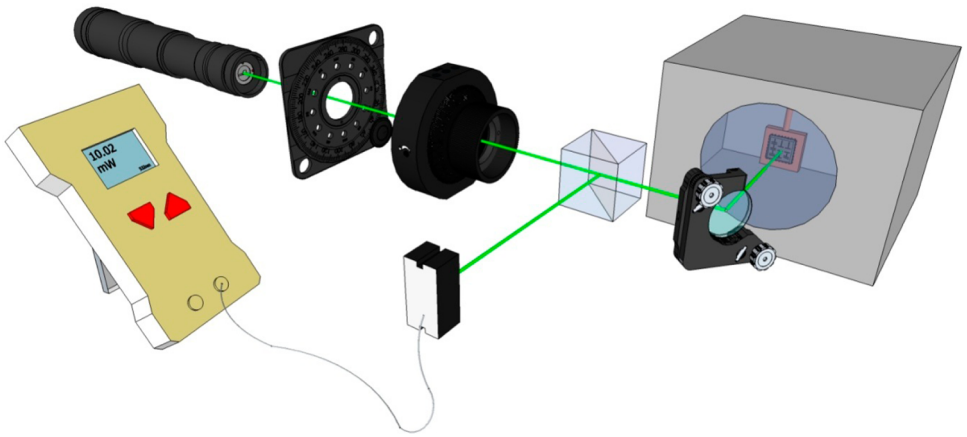

Figure 2. Three-dimensional schematic diagram of the optical setup. To optically excite the NCs, two types of lasers were used: a DPSS CW 1064 nm laser with max power of 150 mW on the sample area (Si-based sensors) and a DPSS CW 532 nm laser with max power of 10 mW on the sample area (Ni-based sensors). The right/left circular polarization for both Hall configurations was generated using a linear polarizer (45°/315°, accordingly), followed by a quarter wave plate. The ensuing laser intensity was monitored by splitting the signal. The gray box represents the cryogenic spectromagPT system used to cool the Ni-based sensor.

In order to obtain highly stable localized magnetization, a thin Co based epitaxial sample was used, namely a Co-based sample. As was already shown in recent papers for Au/Co/Au configuration, a Co layer of 15 Å thickness shows perpendicular magnetization anisotropy with stable, high remanence state.[19,20] This stable remnant magnetization enabled the usage of a light mask and thus locally excited the sample followed by mapping of the magnetization with MFM.

We have recently shown that the AHPA-L molecules sustain their chiral structure with Al_2O_3 on top.[13] The 5 nm Ni thickness was selected in order to achieve maximal perpendicular magnetization. It was previously shown that in a thin Ni layer the Ni film breaks into domains, allowing perpendicular magnetization.[21] The 7 nm Ni sample's magnetization was less stable at RT, unlike the 5 nm Ni sample. The reduced thickness helped the 5 nm sample to achieve a more stable magnetic domain structure at RT.

On top of the thin Ni layer, in all devices, an organic α helix L-polyalanine (AHPA-L) and InAs (CdSe) NCs were adsorbed after several steps. First, the devices were left in absolute ethanol for 20 min; thereafter they were immersed into a 1 mMol ethanol solution of the organic molecule for 3 h. This procedure allows the self-assembled monolayer (SAM) to form a homogeneous, closely packed single layer of molecules. The excess of the organic molecules are removed from the surface by washing the sample with ethanol several times before the samples are dried under nitrogen. Lastly, NCs are attached to the organic layer. For both types of Si-based Hall sensors' configuration experiment, we used InAs NCs with an average size of 5 nm in diameter with an emission peak at 1200 nm. For the Ni-based Hall device, we used core CdSe NCs with an emission peak at 610 nm. Figure 1c shows a scanning electron microscopy (SEM) image with the CdSe NCs' adsorption on top of the AHPA-L molecules. The CdSe NCs were purchased from Sigma-Aldrich Co. LLC. The InAs NCs were synthesized in trioctylphosphine using $InCl_3$ and TMS_3 as precursors, according to the procedure described elsewhere, and they subsequently underwent a size-selection process.[22] Figure 1e shows an absorption spectrum for the InAs and CdSe NCs.

Figure 1a shows a cross section of the shallow Si-based detectors' active area and contacts. Figure 1b shows a top view image of the shallow Si-based sensor, where the conducting channel is along the *X*-axis and the Hall voltage is measured along the *Y*-axis. Here the thin P-doped Si layer conducts between two gold electrodes. Unlike the Ni-based sensor, in both Si-based sensors the Ni layer does not conduct. The energy gap of the InAs NCs (Figure 1e) was chosen to be 1 eV, which is smaller than the smallest gap of the Si channel structure (1.16 eV for bulk Si at RT). Consequently, we can excite the NCs with minimal influence on the Si channel. Previous works show that the NCs' spectra change significantly when self-assembled on a device.[23] Figure 1d shows a scheme of the Ni-based device where no effective adsorption areas were used. This device is much simpler to design and needs only three principal fabrication steps (see Supporting Information Methods).

Both Si-based devices were covered with an Al_2O_3 passivation layer. We have recently shown that the AHPA-L molecules sustain their chiral structure with Al_2O_3 on top.[13] This procedure was done in order to prevent Ni oxidation. Furthermore, stable magnetization at RT was achieved in these devices; therefore the additional capping layer enabled all measurements of these devices to be conducted under ambient conditions. The resistance of these devices did not change before and after the Ni evaporation. The Ni-based device was measured at lower temperatures using a closed loop Oxford spectromagPT system. The Oxford spectromagPT system was also used to induce magnetic fields ranging from 0 to 0.7T. The optical set up was simple and the samples were illuminated through the Crystalline Quartz window of the spectromagPT system.

Figure 2 illustrates the optical setup. To optically excite the NCs, two types of lasers were used: a diode-pumped solid-state continuous-wave (DPSS CW) 1064 nm laser with max power of 150 mW on the sample area (for Si-based sensors) and a DPSS CW 532 nm laser with max power of 10 mW on the sample area (for Ni-based sensor and Co-based sample). The right/left circular polarization illumination (RCP/LCP) for both Hall configurations was achieved using a linear polarizer in the optical path (45° or 315°, accordingly) followed by a quarter wave plate. The ensuing laser intensity was monitored by splitting the signal between an intensity detector and the Hall sensor sample. A simple mechanical shutter was placed along the optical path to compare light and dark measurements.

dx.doi.org/10.1021/nl502391t | *Nano Lett.* XXXX, XXX, XXX−XXX

The absolute response was calculated by subtracting the offset from the RCP (LCP) Hall resistance response normalized by the total. In order to exclude heating effects, most measurements were done using different laser powers in a differential mode, comparing between the responses of different polarizations with the same total power. The differential mode also helps to reduce directed response related to the Si sensors.

The Co-based sample was illuminated for 5 min through an optical transmittance mask that was attached mechanically to the sample. In this sample, the magnetization was expected to be stable long enough to be measured and was mapped using MFM. This measurement showed a highly localized magnetic response (see Results and Discussion).

It was previously shown that when a monolayer of organic molecules and NCs are coupled to a shallow field effect transistor, it is possible to measure charges that accumulate on the surface states of the transistor as a result of charge transfer from the optically excited NCs.[24] The accumulated charges change the electrochemical potential and therefore, they can be measured as a change in the current of the transistor. This yields a variation in the electrostatic potential between the NC's layer and the semiconductor transistor channel underneath, thereby acting as a light-controlled gate.[23] The change in the transistor current is therefore correlated to the NC's coverage and the efficiency of the charge transfer. In this work, we used similar devices and mechanisms for measuring spin transfer. The main difference is the simultaneous measurement of both the Hall resistance, ρ_{xy}, and the longitudinal resistance, ρ_{xx}, since charge transfer occurs via chiral linkers that act as spin filters. The excited electrons oscillate between the NCs and the Ni. Owing to the CISS effect, one type of spin is primarily transferred to the Ni, whereas the opposite spin is reflected back to the NCs inducing spin torque transfer. Consequently, mostly one kind of spin is accumulated on the surface of the sensor in the active adsorption area, creating an effective magnetic field that can be measured by the Hall voltage.

Most Hall sensors have a small offset showing nonzero Hall voltage under dark conditions. We ascribe this small offset to the small asymmetry in the current contacts. In some cases, owing to the Schottky and asymmetric gating effects described above, the offset was changed under illumination. To correct for the offset difference, for each sensor and illumination intensity we took three measurements. We measured the resistance tensor using two circular polarizations and a linear polarization. When only the linear polarization was used, we excited both types of spins at the same ratio and therefore, the spin-related effects are smaller.

If the linker molecules do not have spin selectivity properties, then the linear polarization excitation should result in zero magnetization. The RCP and LCP magnetization should be small and opposite in sign due to the single type of spin excitation in the NCs. However, things are more complicated in the chiral spin filtering case. Here a real nonsymmetric spin torque transfer to the Ni layer is created. In order to evaluate the absolute response manifested as polarized charge transfer in the chiral layer, we used the following concept. In our system, RCP is favored by molecular chirality. Therefore, we denote the unfavorable LCP as -1, which is proportional to the measured Hall voltage with an offset factor, whereas the RCP Hall voltage response is proportional to $+a$ (a is a number larger or equal to 1) with the same offset factor. This yields an absolute relation of 1:a between the LCP and RCP responses. The linear polarization-associated Hall voltage is therefore proportional to $0.5(+a - 1)$ with the same offset. The random offset is the offset of the device under the measured illumination intensity without the spin transport factor. As mentioned above, a small offset is usually introduced to the system due to some asymmetry in the current density. In this case, by using the three magnetization measurements with a linear fit one can calculate the constant offset value and the magnetization ratio.

Results. Figure 3 presents the absolute Hall response for light of two circular polarization directions in the shallow Si-based sensor. All measurements were performed under similar ambient conditions and at RT. In both the right circular polarization (black line) and the left circular polarization (red line), the signal under illumination is compared to the dark signal (alternating every 60 s between dark and light conditions). It is clear that localized magnetization was achieved in both cases. However, whereas the absolute response of the right-handed circular polarization is around $A = 12$ (in some arbitrary unit), the absolute response of the left-handed circular polarization is around $A = 3$. This change in the Hall resistance is 3 orders of magnitude smaller than the sample longitudinal resistance, ρ_{xx}. The large asymmetry ratio of 1:4, measured between the two polarizations, guarantees local magnetization even when the system is excited with non-polarized light. It is also interesting to note that the achieved asymmetry ratio is in agreement with the polarization measured in previous direct transport through chiral molecule experiments.[8]

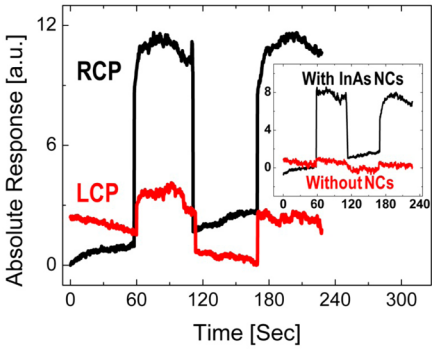

Figure 3. Absolute Hall response for the two circular polarizations as a function of time. All measurements were performed under ambient conditions and at RT. In both the right circular polarization (black line) and the left circular polarization (red line) the signal under illumination is compared to the dark signal (alternating every nearly 60 s as dark−light−dark−light). The inset shows a comparison between the response with and without the InAs NCs. Large magnetization under illumination is achieved only with the NCs.

The Hall coefficient in this case can be evaluated from the density of holes in the channel and the magnetization achieved in the steady state is estimated to be 120G (see the Discussion). The difference between light and dark conditions is repeatable and therefore, noise could be averaged out using the AC measurements. The inset in Figure 3 compares the response for samples with and without the InAs NCs. Large magnetization under illumination is achieved only with the NCs. Without the creation of excitons in the NCs, only a small magnetization effect is measured. The small response obtained for samples without the NCs might be attributed to the recently discovered spinterface effects.[25−27] In order to show the locality of this method, we have fabricated devices with two window sizes: 700 μm × 80 μm and 800 μm × 130 μm and illuminated

dx.doi.org/10.1021/nl502391t | Nano Lett. XXXX, XXX, XXX−XXX

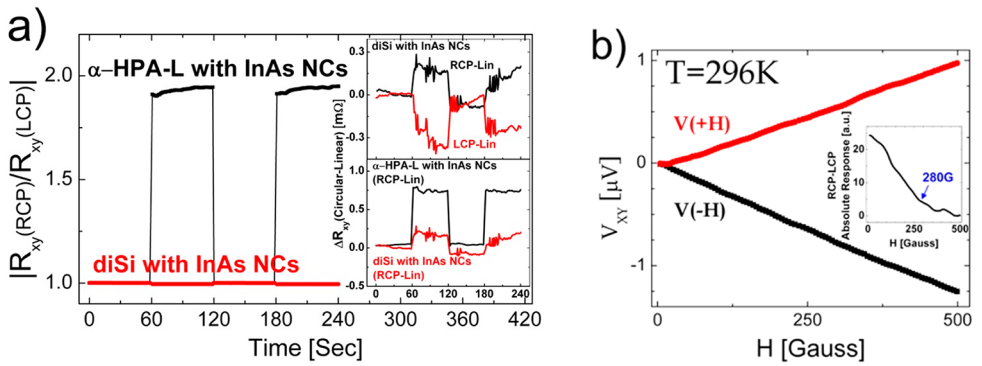

Figure 4. Standard Si-based Hall effect sensor measurements at RT (296 K). (a) Comparison between Hall measurements with InAs NCs linked to chiral AHPA-L molecules and achiral (2-methylene-1,3-propanediyl)bis(trichlorosilane) (disilane) molecules under RCP and LCP illumination. Upper inset: ΔR_{xy} response to illumination of RCP minus linear versus LCP minus linear polarizations of the disilane-prepared sample. Lower inset: ΔR_{xy} response to illumination of RCP minus linear polarizations of the disilane sample compared with the AHPA-L sample. (b) The Si sensors for Hall voltage calibration measurements for the perpendicular (+H) and antiperpendicular (−H) external magnetic field. Inset: RCP minus LCP absolute response under different external magnetic fields that magnetize the Ni layer. When the Ni is magnetized the optical magnetization is less pronounced.. Light-induced magnetic field saturation value of ∼280G is marked in blue.

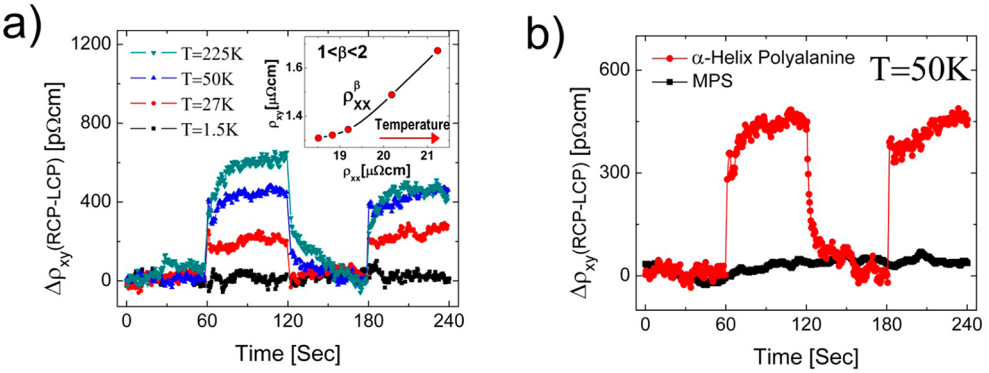

Figure 5. (a) The relative $\Delta\rho_{xy}$ (RCP − LCP) component at different temperatures. Inset: A logarithmic plot of the relations between ρ_{xy} and ρ_{xx} as a function of temperature (the lowest is on the left-hand side) produces a power scale ρ_{xx}^{β} with $1 < \beta < 2$. (b) A reference measurement replacing the chiral layer with achiral 3-mercaptopropyl-trimethoxysilan (MPS) molecules. With MPS no measured difference is seen in the $\Delta\rho_{xy}$ (RCP − LCP), as compared with the large difference measured at 50 K for the chiral layer.

the sample with a spot wider than the active adsorption area size. The total magnetization is similar for both cases. In this sense, using selective adsorption[15] to achieve smaller active area sizes means that the locality of the magnetization induced under illumination and under ambient conditions could be improved. In principle, with selective adsorption for different windows different right or left chiral molecules can be adsorbed, thus creating opposite magnetization under the same unpolarized light illumination.

f4 Figure 4 shows the Hall voltage response using two types of linking molecules covalently bonded on the Ni layer in the standard Si-based sensors. In this case, we used the same sensors and NCs but replaced the chiral AHPA-L molecules with achiral (2-methylene-1,3-propanediyl)bis(trichlorosilane) (di-silane) molecules. The absolute ratio between the RCP and LCP Hall voltage responses for the two molecules is presented in Figure 4a. As expected for the achiral molecules, a small response is achieved that is symmetric for the two polarizations. This is due to the small magnetization induced by exciting one kind of spins in the NCs. The upper inset in Figure 4a shows the two opposite signals measured for the di Silane molecules. The total response of the di Silane is much smaller than the chiral AHPA-L linker's response (Figure 4a bottom inset) because the disilane molecules do not have the spin torque mechanism that exists in the chiral molecules. Figure 4b presents a calibration measurement of the Hall voltage for different directions of external perpendicular magnetic field. This measurement shows that the local light-induced magnetization intensity is around 200G. The inset shows the RCP minus LCP absolute response decay as a function of the external magnetic field. The difference between the response of RCP and LCP decreases with increasing external field. The light-induced saturation magnetic field of ∼280G is marked (see the Discussion).

The Ni-based sensor is a flexible and simpler structure that can be used with a more adaptable choice of NCs. Here only evaporation and lift off are needed and there is no need to choose NCs with a gap smaller than the band gap in the Si structure. Another important advantage of this configuration is that it opens the way to connecting logic structures in series. Figure 5a shows the relative ρ_{xy} component at different f5 temperatures. As can be clearly seen the Hall voltage response increases with temperature. The small signal measured at 1.5K could result from the small AHE in ferromagnetic materials expected at low temperatures.[28,29] At these temperatures, for ferromagnetic films the spin scattering is small and therefore the effective Hall coefficient is small. This result is expected from AHE-predicted behavior. Increasing the temperatures

dx.doi.org/10.1021/nl502391t | Nano Lett. XXXX, XXX, XXX−XXX

while measuring the light versus dark Hall voltage, results in $\Delta\rho_{xy}$ (RCP − LCP) value enhancement. This is true until the Ni demagnetization effect becomes strong. Note the large increase in the asymmetry factor when temperature changes from 1.5 K to 50 K, as compared with the smaller increase for a 50 K to 225 K temperature change. In the inset of Figure 5a, the connection between $\rho_{xy} \propto \rho_{xx}^{\beta}$ is measured for different temperatures. The logarithmic scale fit yields $1 < \beta < 2$, as was previously observed.[30] Figure 5b presents a reference measurement that replaces the chiral layer with achiral 3-mercaptopropyl-trimethoxysilan (MPS) molecules. In this case, no measurable difference is seen in the $\Delta\rho_{xy}$ (RCP − LCP), as compared with the large difference measured at 50 K for the chiral layer.

The local active adsorption areas can obviously create a limited Hall voltage readout that scales down with decreasing size. Therefore, to demonstrate high locality, we used MFM technique. CdSe NCs were linked to AHPA-L molecules that were adsorbed onto a 5 nm thick Au layer located on top of a 1.5 nm thin Co layer. The Co-based sample, where magnetization is stable for long time periods, was grown using a MBE method.[19,20] The epitaxial-grown sample's roughness is very small (Figure 6e). By RCP light excitation through a simple mask, a RT-induced magnetic phase was seen. Using a scanning probe microscope (Dimension 3100 Nanoscope V) mounted with an AFM magnetic tip, we could map the magnetic field

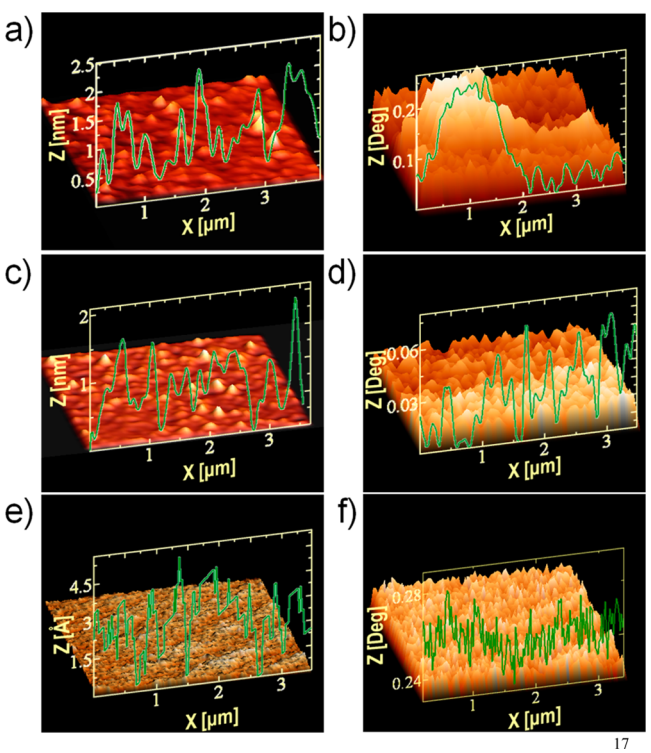

Figure 6. MFM of a Co-based sample after RCP illumination through a light mask. (a) Topographical image of a locally illuminated area reveals CdSe NC adsorption. (b) Magnetic phase image of the same illuminated area displays a highly localized magnetic response. (c) Topographic image of a darkened area during illumination where CdSe NCs can be seen. (d) Magnetic phase image of the same darkened area suggests that no magnetization occurs. (e) Topographic image of an illuminated reference sample without NCs (measured in angstroms). (f) Magnetic phase image of the same illuminated area suggests that no magnetization occurs when there are no NCs.

along the Co sample. Figure 6a,c displays average roughness topography of ∼1.5 nm, although 5 nm NCs were used. This is attributed to the 40 nm magnetic tip that cannot provide topographic resolution on a NC scale for high density of NCs. The MFM technique used a lift mode which combines a topographic image with a magnetic phase image simultaneously. Figure 6 shows the topographic and magnetic measurements of the illuminated area in a sample with molecules and NCs (Figure 6a,b), the dark area in an illuminated sample with molecules and NCs (Figure 6c,d), and an illuminated sample without the NCs (Figure 6e,f).

Discussion. The devices presented here are based on the chiral-induced spin-selectivity effect (CISS).[31] It is clear that the spin filtering of the organic layer is the source of the local magnetization effect and that the NCs are essential for achieving substantial magnetization. The NCs' relevant spin coherence time, T1, at ambient temperatures is longer than 100 ps,[32,33] more than an order of magnitude larger than transport times through the organic chiral molecules.[34,35] The radiative lifetime is in the order of nanoseconds in these systems. Therefore, it is reasonable to assume that the excited state of the spin does not change dramatically before charge transfer occurs. In this case, changes in the Hall voltage between diffracted polarization excitations predominantly originate from the overlap between the excited state and the spin filtering direction. Consequently, an expected magnetization is also probable for nonpolarized light where the excited spin is random, similarly to the linear polarization effect.

In the shallow Si-based sensor, a 4-fold response difference was measured between RCP and LCP light-stimulated polarizations (Figure 3). This ratio was measured in previous works and suggests that a strong spin filtering effect of the AHPA-L chiral molecules exists. In the standard Si-based sensor, a 2-fold difference was measured. We do not fully understand the origin of the smaller selectivity; nevertheless, in both cases the covalently bonded AHPA-L molecules serve as spin torque injectors. Figure 4b inset results provide evidence that the light effect is to induce magnetization in the Ni layer. The difference between the RCP and LCP response decays when we magnetize the Ni layer using an external magnetic field. When the Ni magnetization saturates around 300G, the CISS magnetization cannot be distinguished.

The NCs are excited by the illumination and charges that pass through the chiral layer toward the surface and back to the NCs. The charges' magnetic momentum is aligned parallel or antiparallel to the molecular major axis (perpendicular to the linked channel surface), according to the chiral asymmetry properties of the molecules. When electrons pass between the NCs and the Ni, due to the presence of the chiral potential, one type of spin is primarily transferred to the Ni, whereas the opposite spin is transferred back to the NCs. Therefore, each charge oscillating between the surface and the NCs enhances the Ni magnetization in both directions of the current. In other words, even without charging the surface, the oscillating charges pass a spin torque to the Ni (Figure 1f). One spin orientation is injected into the Ni whereas the opposite is transferred in the opposite direction, generating a spin torque transfer.

For thin ferromagnetic films (5 nm Ni and 1.5 nm Co) the lateral critical current density for switching is around 10^6 A/cm^2.[36,37] Switching gradually the magnetic field by driving magnetic domain walls needs lower critical currents; however, the classical geometries where the current is injected in the plane of the magnetic layers suffer from poor efficiencies for

dx.doi.org/10.1021/nl502391t | Nano Lett. XXXX, XXX, XXX−XXX

this process. Vertical spin transfer mechanism is one of the ways foreseen in driving magnetic domain wall efficiently therefore it is considered for switching of future spintronics memories or registers.[38] The involved current densities are about 100 times smaller than the one commonly observed with in-plane currents, that is, 10^3-10^4 A/cm^2.[39]

Our suggested optical CISS spin torque device is inherently a vertical spin transfer device. Excited electrons can oscillate at a rate of 10^{10} Hz between the ferromagnetic surface state and the NCs transferring a spin torque each oscillating period with current density in one direction of around 10^{-9} A/NC for each NC. The self-assembled monolayer NCs density is around 10^{12} NCs/cm^2. Therefore, our vertical spin torque current density is around 10^3 A/cm^2 which is in the ballpark of existing devices.

Because the Ni demagnetization time is more than 10 orders of magnitude larger than the NCs' demagnetization time, only the NCs' demagnetization time plays a role in the magnetization process. With radiative time of nanoseconds and the high quantum efficiency of the light absorption, more than 10^9 electron spin transfers take place every second. Improved performance may readily be achieved by NCs and molecular length optimization. For the NCs, it is preferable to have a T1 that is short enough (much shorter than the Ni demagnetization time) but longer than the transport time through the chiral molecules. The chiral molecules would benefit from being long, thus enhancing the spin filtering effect.[40] Nonetheless, long chiral molecules will require longer transport time. Consequently, the magnetization will reach saturation at a certain light power level for each system, depending on the different time scales. In addition, the thin Ni layer magnetization could saturate at several tens to a few hundreds Gauss range at RT.[41,42] Indeed, when adding 20% to the of the exciting laser power yielded no change in the measured Hall voltage due to spin. The 5 nm ferromagnetic Ni layer was chosen in order to achieve RT magnetization in thin layers.[43] The conducting Ni layer (7 nm) could enable the use of the Ni magnetization for a series of logic devices. One layer of magnetized Ni could be connected to another ferromagnetic layer through a chiral filter. The total resistance will be modified according to the first and second Ni channel's magnetization, achieving the planar spin logic.

This ferromagnetic Ni-based device also exhibits AHE characteristics, as expected for thin ferromagnetic layers. According to the AHE studies, the impurities scattering are mostly dominant in the sub-4 K regime, which could result in slow spin accumulation. In this region small changes in ρ_{xy} are predicted as well. At higher temperatures, the AHE spin asymmetry mechanisms are stronger (Figure 5) and they include intrinsic, skew scattering, and side-jump contributions. The influence of each of these mechanisms at different temperatures on the AHE is still controversial and is sample specific.[44−48] The inset in Figure 5a shows the empirical power law $\rho_{xy} \propto \rho_{xx}^{\beta}$ measured for thin ferromagnetic layers at the AHE regime. The linear fitting of a logarithmic scale yielded $1 < \beta < 2$, which is in good agreement with theoretical and experimental studies.[30,45,49] These results are the hallmark of the AHE and thus, they provide an indication of the magnetization caused by the ferromagnetic layer. They suggest that a local magnetic field was induced using optical gating without the traditional use of an external magnetic field.

Using the Drude model, the RT 5 nm Ni magnetization of the shallow Si-based sensor can be evaluated. For the Si device the magnetic field is related to the classical Hall coefficient by the following approximation $|B_z| = |((neE_y)/j_x)|$, where n is the density of charge carriers, e is the electron charge, E_y is the electric field, B is the magnetic field, and j_x is the current density. For this device $n \approx 1024$ e/m^3, $E_y \approx 125$ V/m, and $j_x \approx 1.6 \times 10^9$ A/m^2, corresponding to a magnetic field of ∼120G. In the standard Si-based device, the Hall response was also calibrated. Using the linear relation $|(V_{xy}/B_z)| = |(I_{xx}/nte)| \approx 2 \times 10^{-5}$ V/T (as seen in Figure 4b), where $I_{xx} = 10$ mA is the current in the x-direction, $t \sim 250$ nm is the conducting layer thickness, and e is electron charge; the electron density is approximately $n \approx 10^{27}$ e/m^3, which is in good agreement with the expected value for a doping and diffusion processes of a solid source with a saturated solubility concentration of $n \approx 5 \times 10^{26}$ e/m^3. Applying a calibration Hall coefficient value to the measured V_{xy}(RCP − Linear) $\approx 7 \times 10^{-6}$ V yields $B_z \sim 280$G; this corresponds very well to the shallow Si sensors' results and the estimated value for the possible induced magnetic field for thin Ni layers. Figure 6 shows a highly localized magnetization. By illuminating locally down to the minimal optical resolution scale, we can magnetize local optical memory.

Lastly, control over the demagnetization time could be used as a tool to produce strong local magnetization pulses that may be relevant for nuclear magnetic resonance or for designing EPR chips. In this case, the Ni channel could be magnetized in a parallel direction and a pulse of light should create the perpendicular spin torque.

Summary. The above results show that the surface Hall sensor configuration is optimal for measuring spin transfer. The thin ferromagnetic layer on top of the active area of the Hall sensor can be magnetized by transferring spin torque from the NCs through the organic layers, thus creating perpendicular magnetization. Using a chiral layer and selective adsorption, optically induced local magnetization could be achieved in a designed pattern at ambient temperatures. Thus, optically induced local magnetization without the traditional use of a external magnet was achieved. Future applications could be highly localized nanometric spintronic 3D logic devices that enable low power consumption, high data storage density, and cheap fabrication of optically controlled logic units.

■ ASSOCIATED CONTENT

Supporting Information

Shallow and standard Si-based sensors fabrication methods and procedures, Co-based sample fabrication methods and procedures, magnetic hysteresis loop, and domain structure of the Co-based sample. This material is available free of charge via the Internet at http://pubs.acs.org.

■ AUTHOR INFORMATION

Corresponding Author

*E-mail: (Y.P.) paltiel@mail.huji.ac.il.

Author Contributions

The manuscript was written with contributions from all the authors. All authors have approved the final version of the manuscript.

Funding

Funding of this project was done by the Volkswagen Foundation and by Yissum, the I.P. Company of the Hebrew University of Jerusalem.

Notes

The authors declare no competing financial interest.

■ ACKNOWLEDGMENTS

Volkswagen Foundation and by Yissum, the I.P. Company of the Hebrew University of Jerusalem. We would like to thank Yurai Amit and Professor Uri Banin for supplying the InAs NCs. Also to Dr. A. Radko, Ms. N. Mazursky, and Ms. G. Chechelinsky for their devotion and assistance in the sample preparation processes in addition to other staff members of The Center for Nanoscience and Nanotechnology of the Hebrew University of Jerusalem. O.B would also like to thank Mr. A. Neubauer, Mr. E. Cohen, and Mr. I. Eisenberg for their important contributions to this work. Special thanks go to Dr. Z. Paltiel for the remarks and discussions that helped polish this paper.

■ ABBREVIATIONS

RT, room temperature; NC, nanocrystal; AHE, anomalous Hall effect; PECVD, plasma enhanced chemical vapor deposition; AFM, atomic force microscopy; AHPA-L, α helix L-polyalanine; SAM, self-assembled monolayer; SEM, scanning electron microscopy; DPSS CW, diode pumped solid state continuous wave; RCP/LCP, right/left circular polarization; MPS, 3-mercaptopropyl-trimethoxysilan; CISS, chiral induced spin-selectivity effect

■ REFERENCES

(1) Wolf, S. A.; Awschalom, D. D.; Buhrman, R. A.; Daughton, J. M.; Molnár, S. von; Roukes, M. L.; Chtchelkanova, A. Y.; Treger, D. M. *Science* **2001**, *294*, 1488−1495.
(2) Wolf, S. A.; Chtchelkanova, A. Y.; Treger, D. M. *IBM J. Res. Dev.* **2006**, *50*, 101−110.
(3) Lou, X.; Adelmann, C.; Crooker, S. A.; Garlid, E. S.; Zhang, J.; Reddy, K. S. M.; Flexner, S. D.; Palmstrøm, C. J.; Crowell, P. A. *Nat. Phys.* **2007**, *3*, 197−202.
(4) Schmidt, G.; Ferrand, D.; Molenkamp, L. W.; Filip, A. T.; van Wees, B. J. *Phys. Rev. B* **2000**, *62*, R4790−R4793.
(5) Rashba, E. I. *Phys. Rev. B* **2000**, *62*, R16267−R16270.
(6) Ohno, H. *Science* **1998**, *281*, 951−956.
(7) Göhler, B.; Hamelbeck, V.; Markus, T. Z.; Kettner, M.; Hanne, G. F.; Vager, Z.; Naaman, R.; Zacharias, H. *Science* **2011**, *331*, 894−897.
(8) Xie, Z.; Markus, T. Z.; Cohen, S. R.; Vager, Z.; Gutierrez, R.; Naaman, R. *Nano Lett.* **2011**, *11*, 4652−4655.
(9) Yeganeh, S.; Ratner, M. A.; Medina, E.; Mujica, V. *J. Chem. Phys.* **2009**, *131*, 014707.
(10) Medina, E.; López, F.; Ratner, M. A.; Mujica, V. *EPL* **2012**, *99*, 17006.
(11) Gutierrez, R.; Díaz, E.; Naaman, R.; Cuniberti, G. *Phys. Rev. B* **2012**, *85*, 081404.
(12) Gersten, J.; Kaasbjerg, K.; Nitzan, A. *J. Chem. Phys.* **2013**, *139*, 114111.
(13) Dor, O. B.; Yochelis, S.; Mathew, S. P.; Naaman, R.; Paltiel, Y. *Nat. Commun.* **2013**, *4*, 2256.
(14) Valet, T.; Fert, A. *Phys. Rev. B* **1993**, *48*, 7099−7113.
(15) Koslovsky, O.; Yochelis, S.; Livneh, N.; Harats, M. G.; Rapaport, R.; Paltiel, Y. *J. Nanomater.* **2012**, *2012*, 4.
(16) Ramsden, E. *Hall-Effect Sensors: Theory and Application*; Newnes: New South Wales, 2011.
(17) Stiles, M. D.; Zangwill, A. *Phys. Rev. B* **2002**, *66*, 014407.
(18) Ralph, D. C.; Stiles, M. D. *J. Magn. Magn. Mater.* **2008**, *320*, 1190−1216.
(19) Kisielewski, M.; Maziewski, A.; Kurant, Z.; Tekielak, M.; Wawro, A.; Baczewski, L. T. *J. Appl. Phys.* **2003**, *93*, 7628−7630.
(20) Kisielewski, M.; Maziewski, A.; Tekielak, M.; Wawro, A.; Baczewski, L. T. *Phys. Rev. Lett.* **2002**, *89*, 087203.
(21) Kartopu, G.; Yalçın, O.; Choy, K.-L.; Topkaya, R.; Kazan, S.; Aktaş, B. *J. Appl. Phys.* **2011**, *109*, 033909−8.
(22) Guzelian, A. A.; Banin, U.; Kadavanich, A. V.; Peng, X.; Alivisatos, A. P. *Appl. Phys. Lett.* **1996**, *69*, 1432−1434.
(23) Aqua, T.; Naaman, R.; Aharoni, A.; Banin, U.; Paltiel, Y. *Appl. Phys. Lett.* **2008**, *92*, 223112−3.
(24) Neubauer, A.; Yochelis, S.; Popov, I.; Ben Hur, A.; Gradkowski, K.; Banin, U.; Paltiel, Y. *J. Phys. Chem. C* **2012**, *116*, 15641−15645.
(25) Djeghloul, F.; Ibrahim, F.; Cantoni, M.; Bowen, M.; Joly, L.; Boukari, S.; Ohresser, P.; Bertran, F.; Le Fèvre, P.; Thakur, P.; Scheurer, F.; Miyamachi, T.; Mattana, R.; Seneor, P.; Jaafar, A.; Rinaldi, C.; Javaid, S.; Arabski, J.; Kappler, J.-P.; Wulfhekel, W.; Brookes, N. B.; Bertacco, R.; Taleb-Ibrahimi, A.; Alouani, M.; Beaurepaire, E.; Weber, W. *Sci. Rep.* **2013**, *3*, 1272.
(26) Steil, S.; Großmann, N.; Laux, M.; Ruffing, A.; Steil, D.; Wiesenmayer, M.; Mathias, S.; Monti, O. L. A.; Cinchetti, M.; Aeschlimann, M. *Nat. Phys.* **2013**, *9*, 242−247.
(27) Goldsmith, M.-R.; George, C. B.; Zuber, G.; Naaman, R.; Waldeck, D. H.; Wipf, P.; Beratan, D. N. *Phys. Chem. Chem. Phys.* **2006**, *8*, 63−67.
(28) Miyasato, T.; Abe, N.; Fujii, T.; Asamitsu, A.; Onoda, S.; Onose, Y.; Nagaosa, N.; Tokura, Y. *Phys. Rev. Lett.* **2007**, *99*, 086602.
(29) Nagaosa, N.; Sinova, J.; Onoda, S.; MacDonald, A. H.; Ong, N. P. *Rev. Mod. Phys.* **2010**, *82*, 1539−1592.
(30) Ye, L.; Tian, Y.; Jin, X.; Xiao, D. *Phys. Rev. B* **2012**, *85*, 220403.
(31) Naaman, R.; Waldeck, D. H. *J. Phys. Chem. Lett.* **2012**, *3*, 2178−2187.
(32) Zhang, Z.; Jin, Z.; Ma, H.; Xu, Y.; Lin, X.; Ma, G.; Sun, X. *Phys. E* **2014**, *56*, 85−89.
(33) Warner, M.; Din, S.; Tupitsyn, I. S.; Morley, G. W.; Stoneham, A. M.; Gardener, J. A.; Wu, Z.; Fisher, A. J.; Heutz, S.; Kay, C. W. M.; Aeppli, G. *Nature* **2013**, *503*, 504−508.
(34) Brabec, C. J.; Zerza, G.; Cerullo, G.; De Silvestri, S.; Luzzati, S.; Hummelen, J. C.; Sariciftci, S. *Chem. Phys. Lett.* **2001**, *340*, 232−236.
(35) Wang, Y.; Hang, K.; Anderson, N. A.; Lian, T. *J. Phys. Chem. B* **2003**, *107*, 9434−9440.
(36) Jiang, Y.; Nozaki, T.; Abe, S.; Ochiai, T.; Hirohata, A.; Tezuka, N.; Inomata, K. *Nat. Mater.* **2004**, *3*, 361−364.
(37) Liu, L.; Moriyama, T.; Ralph, D. C.; Buhrman, R. A. *Appl. Phys. Lett.* **2009**, *94*, 122508.
(38) Chanthbouala, A.; Matsumoto, R.; Grollier, J.; Cros, V.; Anane, A.; Fert, A.; Khvalkovskiy, A. V.; Zvezdin, K. A.; Nishimura, K.; Nagamine, Y.; Maehara, H.; Tsunekawa, K.; Fukushima, A.; Yuasa, S. *Nat. Phys.* **2011**, *7*, 626−630.
(39) Metaxas, P. J.; Sampaio, J.; Chanthbouala, A.; Matsumoto, R.; Anane, A.; Fert, A.; Zvezdin, K. A.; Yakushiji, K.; Kubota, H.; Fukushima, A.; Yuasa, S.; Nishimura, K.; Nagamine, Y.; Maehara, H.; Tsunekawa, K.; Cros, V.; Grollier, J. *Sci. Rep.* **2013**, *3*, 1829.
(40) Morton, J. J. L.; Tyryshkin, A. M.; Ardavan, A.; Porfyrakis, K.; Lyon, S. A.; Briggs, G. A. D. *J. Chem. Phys.* **2006**, *124*, 014508.
(41) Bochi, G.; Ballentine, C. A.; Inglefield, H. E.; Thompson, C. V.; O'Handley, R. C.; Hug, H. J.; Stiefel, B.; Moser, A.; Güntherodt, H.-J. *Phys. Rev. B* **1995**, *52*, 7311−7321.
(42) Song, X.; Fan, J.; Zhang, X.-G.; Zhang, D. *Phys. Lett. A* **2010**, *374*, 3881−3886.
(43) Bochi, G.; Hug, H. J.; Paul, D. I.; Stiefel, B.; Moser, A.; Parashikov, I.; Güntherodt, H.-J.; O'Handley, R. C. *Phys. Rev. Lett.* **1995**, *75*, 1839−1842.
(44) Karplus, R.; Luttinger, J. M. *Phys. Rev.* **1954**, *95*, 1154−1160.
(45) Kooi, C. *Phys. Rev.* **1954**, *95*, 843−844.
(46) Carr, W. J. *Phys. Rev.* **1958**, *109*, 1971−1976.
(47) Smit, J. *Physica* **1958**, *24*, 39−51.
(48) Berger, L. *Phys. Rev. B* **1970**, *2*, 4559−4566.
(49) Kondo, J. *Prog. Theor. Phys.* **1962**, *27*, 772−792.